Phytomedicine 97 (2022) 153920

Contents lists available at ScienceDirect

Phytomedicine

journal homepage: www.elsevier.com/locate/phymed

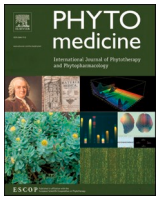

Sheng Mai San ameliorated heat stress-induced liver injury via regulating energy metabolism and AMPK/Drp1-dependent autophagy process

Xiaosong Zhang, Yaqian Jia, Ziwen Yuan, Yanqiao Wen, Yahui Zhang, Jianmin Ren, Peng Ji, Wanling Yao, Yongli Hua, Yanming Wei *

Institute of Traditional Chinese Veterinary Medicine, College of Veterinary Medicine, Gansu Agricultural University, Lanzhou, Gansu 730070, China

ARTICLE INFO

Keywords:
Heat stress
Sheng Mai San
Liver injury
Energy metabolism
Oxidative stress
Autophagy

ABSTRACT

Background: Liver damage is one of the most common complications in humans and animals after heat stress (HS). Sheng Mai San (SMS), a traditional Chinese medicine prescription that originated in the Jin Dynasty, exert a therapeutic effect on HS. However, how SMS prevents liver injury after heat exposure remains unknown.
Purpose: This study aimed to investigate the pharmacological effect and molecular mechanisms of SMS on HS-induced liver injury.
Study design: A comprehensive strategy via incorporating pharmacodynamics, targeted metabolomics, and molecular biology technology was adopted to investigate energy metabolism changes and the therapeutic mechanisms of SMS in HS-induced rat liver injury.
Methods: First, *Sprague-Dawley* rats were subjected to HS (38 °C/ 75% RH/ 2 h/ day) for 7 consecutive days to establish the HS model, and SMS was given orally for treatment 2 h before heat exposure. Thereafter, liver function and pathological changes in liver tissue were evaluated. Finally, the underlying mechanisms of SMS were determined using targeted energy metabolomics to comprehensively analyze the metabolic pathways and were further verified through Western-blot and qRT-PCR assays.
Results: Our results showed that SMS alleviated HS-induced liver dysfunction by reducing the alanine aminotransferase (ALT), aspartate aminotransferase (AST), and AST/ALT ratios in serum and improving hepatic pathological damage. Meanwhile, SMS suppressed inflammatory response, oxidative injury, and overexpression of heat shock proteins in liver tissue after heat exposure. With the help of targeted energy metabolomics, we found that SMS could effectively regulate glycolysis and tricarboxylic acid (TCA) cycle to relieve energy metabolism disorder. Furthermore, we confirmed that SMS can facilitate the phosphorylation of AMP-activated protein kinase (AMPK) to maintain mitochondrial homeostasis through a dynamin protein 1 (Drp1)-dependent mitophagy process.
Conclusion: On the basis of energy metabolomics, the present study for the first time systematically illustrated the protective effect of SMS on HS-induced liver injury, and preliminarily confirmed that an AMPK-mediated Drp1-dependent mitophagy and mitochondria rebuilding process plays an important role in SMS intervention on HS-induced rat liver. Together, our study lends further support to the use of SMS in treating HS condition.

Introduction

As global warming worsens, extreme high temperature is becoming an increasing threat not only for human health worldwide but also for livestock production (Li et al., 2020). Long-term exposure to high temperatures exceeding 40 °C increases core body temperature (Tc) and

Abbreviations: ALT, alanine aminotransferase; AST, aspartate aminotransferase; Cytc, cytochrome c; CAT, catalase; Drp1, dynamin-related protein 1; HPLC, high performance liquid chromatography; HS, heat stress; HSP, heat shock protein; HCA, hierarchical cluster analysis; HRP, horseradish peroxidase; H&E, Hematoxylin-Eosin; TNF, tumor necrosis factor; MDA, malondialdehyde; MPO, myeloperoxidase; MRM, Multiple Reaction Monitoring; NAC, N-acetyl-L-cysteine; PAS, periodic acid-Schiff; PCA, principal component analysis; QC, quality control; qRT-PCR, quantitative real-time polymerase chain reaction; SMS, Sheng Mai San; SIRS, systemic inflammatory response; SOD, superoxide dismutase; TCA, tricarboxylic acid; Tc, core body temperature; UPLC–MS/MS, ultra–performance liquid chromatography–tandem mass spectrometry; 8-OHDG, 8-hydroxydeoxyguanosine.

* Corresponding author.
E-mail address: weiym@gsau.edu.cn (Y. Wei).

https://doi.org/10.1016/j.phymed.2021.153920
Received 27 September 2021; Received in revised form 21 December 2021; Accepted 30 December 2021
Available online 31 December 2021

causes stress (Stim, 1994). In domesticated livestock, heat stress (HS) causes low fertility, reduced animal welfare, and increased susceptibility and mortality to disease in extreme cases (Gonzalez-Rivas et al., 2020). Moreover, it is generally accepted that HS leads to many unfavorable effects in terms of physiological and behavioral disturbances, such as heat stroke, nerve damage, immune disorders, and multi-organ dysfunction (Bouchama and Knochel, 2002). The liver plays an important role in executing essential functions such as energy metabolism homeostasis, synthesis of bile, storage of glycogen, and removal of toxins. Liver damage and failure are well-documented complications in humans and animals after HS. Emerging evidence suggests that liver injury is absent at the onset of HS, but presents during HS recovery in patients and animal models (Davis et al., 2017; Geng et al., 2015). The exact mechanisms that lead to hepatic damage in HS remain unclear, but accumulating *in vitro* and *in vivo* investigations have demonstrated that energy metabolism disorder and systemic inflammatory response (SIRS) play a critical role in cellular injury after heat exposure (Davis et al., 2017). Lowering core body temperature and supporting organ system function are the primary goals against HS in humans and animals. As an intervention, various physiotherapies and drugs have been used to ameliorate HS-induced insult, such as hyperbaric oxygen therapy, dexamethasone, and kynurenic acid, which reduce free radical generation and SIRS (Gupta et al., 2021). Owing to the unmet need for HS control in modern medicine, clinicians have begun to consider the possible role of traditional Chinese medicine (TCM) in the prevention and treatment of HS, and a number of basic and clinical studies in this field have drawn increasing attention.

Sheng Mai San (SMS), described in a classic Chinese medicine literature of the Jin Dynasty (*Yi Xue Qi Yuan*, compiled by Yuansu Zhang), consists of three herbal components, the dried root of *Panax ginseng* C.A. Mey. (Ren Shen), the dried root tuber of *Ophiopogon japonicas* (Thunb.) Ker-Gawl. (Mai Dong), and the dried ripe fruit of *Schisandra chinensis* (Turcz.) Baill. (Wu Wei Zi), is routinely being used for treating chronic bronchitis, liver failure, myocardial ischemia, and shock in clinics (Zhang et al., 2018; Zheng et al., 2011). Previous studies demonstrated that SMS effectively suppressed cerebral ischemia and renal damage during heat stroke by reducing inflammation response and oxidative stress (Lee et al., 2005; Wang et al., 2005b). Although considerable evidence has shown the pharmacological efficacy of SMS during heatstroke, whether prior administration of SMS can attenuate inflammatory cytokines and oxidative stress in HS-induced liver injury remains unknown.

Metabolomics, a branch of systems biology, describes the biological, physiological, and pathological states in living systems in response to exogenous stimulation (Nicholson et al., 1999). A combination of system biology and classical molecular biology could be comprehensively efficient for corresponding pharmacological targets. Previous metabolomics, proteomics, and transcriptomic profiles indicate that energy crisis and oxidative stress are viable metabolic indicators for predicting HS-induced injury and recovery, and the liver is one of the target organs (Ippolito et al., 2014). Mitochondria are dynamic organelles that constantly change their morphology through fission and fusion to maintain energy requirement in organisms. Dynamin-related protein 1 (Drp1) is a major regulator of mitochondrial fission. Recent studies indicated that autophagy facilitates mitochondrial rebuilding after acute HS via a Drp1-dependent process (Chen et al., 2021). Furthermore, AMP-activated protein kinase (AMPK) acts as a central metabolic regulator and plays a key role in energy balance, which promotes mitophagy to remove defective mitochondria to deal with oxidative stress damage (Garcia and Shaw, 2017; Hu et al., 2021). Thus, a combination of targeted energy metabolomics and mitochondria dynamics is an interesting avenue of study.

Considering that previous investigations indicate the protective effect of SMS on HS-induced damage, we hypothesized that an AMPK-mediated energy homeostasis and mitochondria rebuilding pathway might be involved in SMS treatment of HS-induced liver injury. Therefore, by employing a HS-induced rat liver injury model, we systematically investigated the therapeutic effects of SMS on HS-induced liver insults from an energy metabolism and mitochondria homeostasis perspective. Overall, the principal aim of the study was to explore the role and regulatory mechanism of SMS in the response to liver damage after heat exposure and provide theoretical basis for future applications.

Materials and methods

Animals and ethical statement

Specific Pathogen Free (SPF) grade *Sprague Dawley* (SD) male rats (six weeks old, body weight (b. w.) 180 ± 20 g) were purchased from the Experimental Animal Center of the Lanzhou Veterinary Research Institute of the Chinese Academy of Agricultural Sciences [SCXK (Gan) 2020–0002]. All the animal were housed in the animal center of College of Veterinary Medicine of Gansu Agricultural University, and they received humane care in accordance with the "Guidelines for the Management and Use of Laboratory Animals" (Ministry of Science and Technology of China, 2006). All studies were conducted in line with the China Physiological Society's Guiding Principles in the care and Use of Animals and with the approval of the Animal Care Committee of Gansu Agricultural University (NO. GSAU-ETH-VMC-2020-003). The animals were raised in conventional facility (12 h light/dark cycle, 23 ± 1 °C, 45 ± 5% relative humidity, free access to distilled water and commercial rodent food *ad libitum*) for one week before experiment.

Preparation and quality control of SMS

Panax ginseng C.A. Mey. (Ren Shen, batch number: 190802, collected in Jilin, China), *Ophiopogon japonicas* (Thunb.) Ker-Gawl. (Mai Dong, batch number: 200101, collected in Sichuan, China), *and Schisandra chinensis* (Turcz.) Baill. (Wu Wei Zi, batch number: 191001, collected in Heilongjiang, China) were purchased from Yellow River Chinese Medicine Co. Ltd (Lanzhou, Gansu, China). These voucher specimens, which deposited in Traditional Chinese Veterinary Medicine Laboratory of Gansu Agricultural University (GSAU20200601), were authenticated by Professor Yanming Wei (College of Veterinary Medicine, Gansu Agricultural University, Lanzhou, China) according to Chinese Pharmacopoeia 2020 edition. Following the ancient documents, SMS samples were prepared with *Panax ginseng* C. A. Mey., *Ophiopogon japonicus* (l. f) Ker-Gawl., and *Schisandra chinensis* (Turcz.) Baill. at a weight ratio of 3:3:2(*w/w/w*). These three herbs were mixed with 10 times distilled water (*v/w*) and soaked for 30 min. Then, the mixture was extracted by refluxing for 1 h. The residue was then refluxed with 8 times distilled water (*v/w*) for 40 min and subsequently filtered through four layers of gauze. Then, the two filtrates were mixed together and concentrated to the relative density of 1.00 g/mL with rotary evaporation under vacuum at 60 °C. After further freeze-drying, SMS decoction powder was obtained (yield: 57.67%) (Chen et al., 2016; Zhang et al., 2016). In *in vivo* experiment, SMS decoction powder was dissolved in distilled water to a concentration of 1.00 g/mL (calculating with raw herbs), and stored at 4 °C before the experiment.

For quality control analysis, the freeze-dried SMS decoction powder was immersed in 25 mL of methanol (100 mg/mL), extracted for 40 min in ultrasonic vibration machine, and centrifuged at 10,000 rpm for 10 min at 4 °C. Afterward, the filtrate was passed through a 0.22 μm syringe filter to carry out HPLC analysis. Reference standards (purity ≥ 98%) of ginsenoside Rb1 (CAS: 41753–43–9), ginsenoside Rh1 (CAS: 63223–86–9), ginsenoside Rg3 (CAS: 14197–60–5), ophiopogonin D (CAS: 41753–55–3), ruscogenin (CAS: 472–11–7) and schisandrin A (CAS: 61281–38–7) were purchased from Nanjing Yuanzhi Biotechnology Co., Ltd (Nanjing, China). The quality of samples was analyzed with an Agilent 1260 HPLC system (Agilent Technologies, Atlanta, GA, USA). Chromatographic separations were carried out on an Agilent ZORBAX SB-C_{18} column (4.6 × 250 mm, 5 μm) at 25 °C with flow rate of

1.0 mL/min. The mobile phase consisted of 0.1% aqueous phosphoric acid (A) and acetonitrile (B). The mobile phase with a gradient elution program set as follows: 0–10 min, 5% – 15% B; 10 – 35 min, 15% – 35% B; 35 – 40 min, 35% – 45% B; 40 – 50 min, 45% – 50% B; 50 – 85 min, 50% – 65% B. The injection volume was 20 μL, and the ultraviolet detection wavelength was set as 203 nm.

HS model preparation and treatment

Experiment 1: To detect the severe liver injury time point associated with HS, the rats were randomized into six groups (n = 8/group), including control group and five time point groups (0, 3, 6, 9, and 12 h). Before heat exposure, the body weight and temperature were measured. Body temperature was monitored using a rectal thermometer which was inserted 2 cm into the rectum. To induce HS, the animals were placed in a prewarmed incubator that was exposed to HS (38 ± 1 °C, 75 ± 5% relative humidity, AM 10:00 – 12:00, 2 h/day) for 7 consecutive days. The animals were fasted and denied water during the period of HS. Immediately after HS, the rats were removed from the climate chamber, and weighed, and their body temperature was measured. Then, they were returned to the original environment (23 ± 1 °C, 45 ± 5% relative humidity) with *ad libitum* access to food and water. After the last heat exposure, the treated rats were then allowed to recover for 0, 3, 6, 9, and 12 h in conventional environment before sacrifice.

Experiment 2: To investigate the protective effects of pre-treatment with SMS against HS-induced liver damage, the rats were randomly assigned into six groups (n = 8/group): control group, HS group, SMS-H group, SMS-M group, SMS-l group and N-acetyl-l-cysteine (NAC) group. The clinical dosage of SMS was 24 g: 9 g for *Panax ginseng* C. A. Mey., 9 g for *Ophiopogon japonicus* (l. f) Ker-Gawl., and 6 g for *Schisandra chinensis* (Turcz.) Baill., respectively. In this study, medium dosage of SMS was administered at a normal dosage corresponding to its human clinical dosage. The dosage of SMS is calculated by the following equation: $D_m = D_h / W \times F$ (D_m is the administered dosage of SMS for rat in the work, D_h is the clinical dosage of SMS, W is human weight set as 60 kg, F is the dosage conversation factor of 6.3 between rat and human). Thus, the medium dosage of SMS (SMS-M, 2.52 g/kg/day) can be calculated in our study. High dosage of SMS (SMS-H, 5.04 g/kg/day) was twice the dosage of SMS-M, and low dosage of SMS (SMS-lL, 1.26 g/kg/day) was half the dosage of SMS-M. The SMS-treated rats were intragastrically administered with the corresponding dosage of SMS 2 h before heat exposure for 7 consecutive days. NAC can inactivate the activity of oxidative metabolites, the structural stability of cell membrane and intracellular membrane, stable intracellular enzyme and protein function. Thus, it was used as a positive control drug in the research. NAC was administrated intragastrically at a dosage of 150 mg/kg/day according to previous research (Yang et al., 2018). Control and HS group rats were provided an equal volume of physiological saline. The selection of sacrifice-time points was primarily based on Experiment 1, in which rat HS induced liver damage state. The experimental design is summarized in Fig. 1.

Liver function test

At the end of the experiment, the rats were anesthetized by intraperitoneal injection of 10% chloral hydrate. Blood was collected from the abdominal aorta (non-anticoagulant vacuum blood collection tubes). After 2 – 4 h standing at room temperature, the blood samples were centrifuged at 3000 rpm/min for 10 min, and the supernatant was stored at −80 °C for further use. Serum alanine transaminase (ALT), aspartate transaminase (AST) and AST/ALT ratio were determined using commercial assay kits according to the manufacturer's instructions (Nanjing Jianchen Bioengineering Institute, Nanjing, China).

Histology and ultra-structural analysis of rat liver by transmission electron microscopy (TEM)

The livers of all rats were excised rapidly and placed in ice-cold PBS to remove residual blood. Thereafter, they were fixed in 10% formalin (in pH 7.4 PBS). Paraffin embedded liver tissues were sectioned at 4 μm thickness and stained by Hematoxylin-Eosin (H&E). Histopathological scoring was performed in accordance with previously described methods under light microscopy (Olympus, Japan), including six parameters: cytoplasmic color fading, vacuolization, nuclear consideration, nuclear fragmentation, nuclear fading, and erythrocyte stasis. Each parameter was scored according to the percentage of cells per 10 microscopic fields (200 ×): 0 = 0%, 1 = 0% – 10%, 2 = 10% – 50%, 3 = 50% – 100%. The histopathological scores were reported as the sum of the individual values (Heijnen et al., 2003). PAS (periodic acid-Schiff) stain was used in the demonstration of hepatocellular glycogen stores according to previous study (Fu and Campbell-Thompson, 2017). For TEM analysis, fresh liver tissues were quickly cut into 1 – 2 mm^2 size and fixed with 2.5% glutaraldehyde for 24 h (pH=7.4, 4 °C). The tissues were post-fixed in 1% OsO4 for 2 h at room temperature and then dehydrated in graded series of acetone. Epoxy resin-embedded tissues were sectioned at 0.5 μm thickness and stained with uranyl acetate and lead citrate. The ultrastructure of liver tissue was observed by TEM (JEM-1400Plus, Tokyo, Japan).

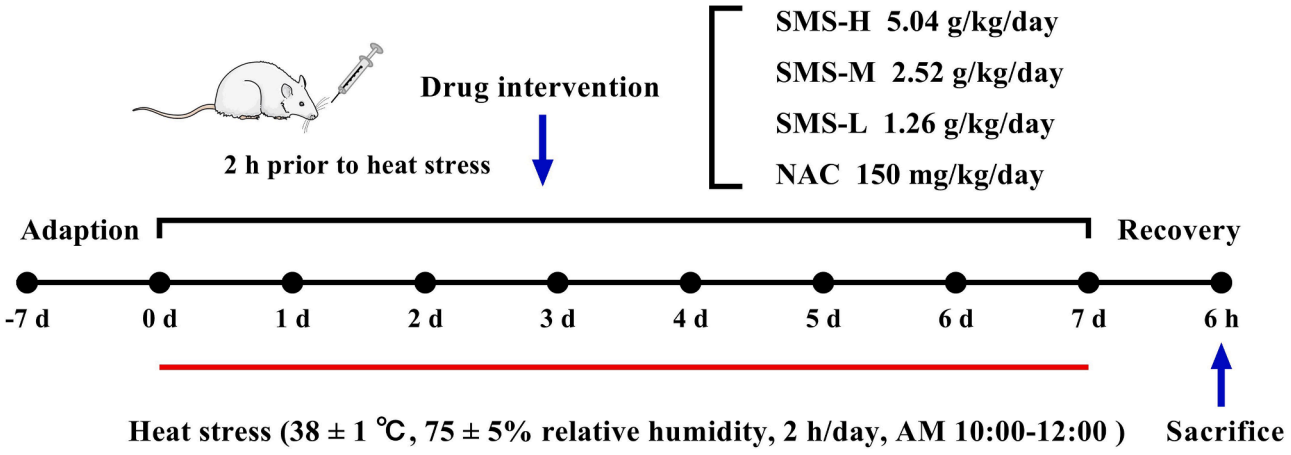

Fig. 1. Study design. Experiments were conducted over 14 d, including an acclimatization period of 7 d. Forty-eight male *Sprague Dawley* rats were randomly assigned to one of six groups (n = 8). Rats were administered with the corresponding dosage SMS at 2 h before heat exposure for 7 consecutive days (i.g.). At the end of the experiment, rats were sacrificed according to animal use guidelines. SMS-H, heat stress + SMS high-dose group; SMS-M, heat stress + SMS medium-dose group; SMS-l, heat stress + SMS low-dose group; NAC, heat stress + N-acetyl-l-cysteine group.

Measurement of antioxidant enzyme activities in liver tissue

Frozen liver tissue was homogenized in ice-cold PBS, and homogenate was centrifuged at 5000 g for 15 min at 4 °C. 8-hydroxydeoxyguanosine (8-OHDG) malondialdehyde (MDA), glutathione (GSH), superoxide dismutase (SOD), and catalase (CAT) were measured using commercial kits according to the manufacturer's instructions (Nanjing Jianchen Bioengineering Institute, Nanjing, China). MDA content was measured with thiobarbituric acid (TBA) reaction at 532 nm. The content of GSH was analyzed with DTNB reaction at 405 nm. SOD levels were determined by measuring the absorbance at 450 nm. CAT activity was determined by measuring the consumption of H_2O_2 at 405 nm. Protein quantification was performed by BCA protein assay kit (Solarbio, Beijing, China). All results were normalized to total protein concentration in each sample.

Targeted metabolomic analysis

In our study, 40 key metabolites involved in the tricarboxylic acid cycle (TCA cycle), glycolytic pathway, pentose phosphate pathway, oxidative phosphorylation and corresponding cofactors were detected simultaneously by ultra-performance liquid chromatography-tandem mass spectrometry (UPLC-MS/MS).

Preparation of liver metabolomic samples

Frozen liver samples (100 mg) were homogenized with 200 μL of pre-chilled distilled water and then added to 800 μL of pre-chilled methanol: acetonitrile (1:1, *v/v*). After being vortexed, the mix solution was sonicated for 60 min in an ice bath and then incubated at −20 °C for 1 h to settle protein. Subsequently, the solution was centrifuged at 16,000 rpm at 4 °C for 20 min. An internal standard Succinate-d6 was added to the supernatant, freeze-dried and stored at −80 °C. The dry residue was diluted with 100 μL of aqueous acetonitrile (1:1, *v/v*) and centrifuged at 16,000 rpm at 4 °C for 20 min for UPLC–MS/MS analysis.

UPLC–MS/MS global profiling of liver metabolites

UPLC–MS/MS analysis was carried out with a Nexera X2 LC-30AD UHPLC system (Shimadzu, Kyoto, Japan), coupled to a 5500 QTRAP mass spectrometer (AB SCIEX, Toronto, Canada). A 5 μL sample was loaded by the autosampler at 4 °C. The separations of all liver samples were performed on a ACQUITY UPLC BEH Amide column (2.1 mm × 100 mm, 1.7 μm, column temperature: 40 °C, flow rate: 300 μL/min, Waters, Milford, USA). The linear gradient mobile phase was composed of (A) 5% aqueous acetonitrile (*v/v*) and (B) 95% aqueous acetonitrile (*v/v*). Moreover, (A) and (B) contain 10 mM ammonium acetate and have a pH=9. The optimized chromatographic gradient elution was set as follows: 0–2 min (95% B); 2–9 min (95%–70% B); 9–10 min (70% – 30% B); 10–11 min (30% B); 11–11.5 min (30%–95% B); 11.5–15 min (95% B). The mass spectrometer parameters were set as follows: ion spray voltage (ISVF): positive mode (ESI+) at 5500 V and negative mode (ESI-) at 4500 V; curtain gas (CUR), nebulizer gas (GS I), and auxiliary gas (GSA II) were set at 35, 40 and 50 psi; source temperature was set at 550 °C. A specific set of Multiple Reaction Monitoring (MRM) transitions was monitored for each period according to the metabolites eluted within this period.

Targeted metabolites analysis

The chromatographic peak areas and retention time were acquired and evaluated via MultiQuant software (AB SCIEX, Toronto, Canada). Peak detection and alignment across all samples were performed with reference to their corresponding standard substances (all standards were purchased from Sigma-Aldrich, St. Louis, USA and Shanghai yuanye Bio-Technology Co., Ltd, Shanghai, China). The chromatographic peak areas were normalized by the internal standard Succinate-d6. To ensure system stability and repeatability, variations in retention time and peak areas of extracted ions should be validated with a quality control (QC) sample (a composite of equal volume from 32 real samples). The acceptable standard of instrument stability and method reproducibility is that the relative standard deviations (RSDs) of peak areas should be less than 30%. Multivariate statistical analysis of principal component analysis (PCA) was carried out by SIMCA-P 14.0 version (Umetrics, Umea, Sweden). All differentially expressed energy metabolites between two groups were confirmed by using *t*-test with the critical *P*-value set to 0.05.

Quantitative real-time polymerase chain reaction (qRT-PCR)

Total RNAs were isolated from frozen tissues (50–100 mg) using TriQuick reagent (Solarbio, Beijing, China) according to the manufacturer's instructions. Double-stranded cDNA was synthesized from 3 μg of total RNA with TransScript® One-Step gDNA Removal and cDNA Synthesis SuperMix Kit (TransGen Biotech, Beijing, China). Real-time PCR analysis was performed by using ChamQ Universal SYBR qPCR Master Mix Kit (Vazyme, Nanjing, China) and the following primer sequences (Supplementary Table S1). All samples were run in triplicate and underwent 40 amplification cycles on a Roche Applied Science LightCycler ® 96 Instrument (Roche, Basel, Switzerland). The $2^{-\Delta\Delta Ct}$ method was employed to analyze relative gene expression, using β-actin as the endogenous reference gene for each sample.

Subcellular fraction and western blot (WB) analysis

Frozen liver tissue was homogenized in RIPA lysis buffer (Solarbio, Beijing, China) and then total protein was extracted from this homogenate with the addition of complete protease inhibitors and phosphatase inhibitors, and centrifuged at 15,500 g for 10 min. Cytosol and mitochondria fractions were isolated using the Tissue Mitochondria Isolation Kit (Beyotime, Beijing, China) according to the manufacturer's protocol. Protein quantification was performed by BCA protein assay kit (Solarbio, Beijing, China). Samples containing equal amounts of protein were loaded into polyacrylamide gels and separated by 10% or 12% sodium dodecyl sulfate-polyacrylamide (SDS -PAGE) (Bio-Rad Laboratories). Then transferred to 0.22 μm PVDF membrane (Millipore, MA, USA). After blocking in Tris-buffered saline containing 0.1% Tween-20 (TBST) with 5% BSA for 2 h at room temperature, membranes were incubated overnight at 4 °C with specific primary antibodies: anti-p-AMPK alpha^{Thr172} (CST, 2535, 1:1000), anti-AMPK alpha (CST, 5831s, 1:1000), anti-p-Drp1^{Ser616} (CST, 3455s, 1:1000), anti-Drp1 (CST, 8570s, 1:1000), anti-CytC (CST, 11940s, 1:1000), anti-LC3B (Abcam, ab192890, 1:2000), anti-SQSTM1/p62 (Proteintech, 18420-1-AP, 1:2000), COXIV (Proteintech, 11242-1-AP, 1:5000), and β-actin (Proteintech, 20-536-1-AP, 1:5000). Afterward, membranes were washed and incubated with horseradish peroxidase (HRP) -conjugated Affini-Pure Goat Anti-Rabbit IgG (Proteintech, SA00001-2, 1:8000) for 1 h at room temperature. The blot was visualized by adding ECL Plus Western blotting detection regent (Vazyme, Nanjing, China), and image acquisition was performed using the Amersham Imager 600 chemiluminometer (GE Healthcare Bio-Sciences AB, Sweden). Densitometry was calculated by Image J software.

Statistical analysis

Statistical analysis was performed with SPSS version 26.0 program package (IBM, Armonk, NY, USA). All data were presented as mean ± standard error of mean (SEM). The difference between two groups was tested by Student's *t*-test. Statistical comparison of more than two groups was performed using one-way analysis of variance (ANOVA) with LSD and Turkrey's post-hoc analysis. All the figures presented in this paper were created using GraphPad Prism (version 9.0, GraphPad Software, La Jolla, CA, USA). Statistical significance was considered at $P < 0.05$.

Results

Quality control analysis of sms using HPLC

The main chemical components of SMS were characterized by HPLC for quality control before the *in vivo* experiment. The HPLC chromatogram has been presented of the SMS decoction powder were chemically identified by comparing the retention time and UV spectrum with those of reference standards (ginsenoside Rb1, ginsenoside Rh1, ginsenoside Rg3, ophiopogonin D, ruscogenin and schisandrin A) (Fig. 2). The linear relationship of each compound was good within the corresponding detection concentration range (Supplementary Table S2). The results of precision, stability, sample recovery rate and repeatability test showed that the RSD values were less than 5% (Supplementary Tables S3–S6). The concentration of six major compounds (ginsenoside Rb1, ginsenoside Rh1, ginsenoside Rg3, ophiopogonin D, ruscogenin and schisandrin A) in SMS decoction powder, were 76.6675 ± 8.4606, 461.1041 ± 8.4606, 298.3461 ± 1.4827, 52.7504 ± 9.3551, 134.7861 ± 2.4161, and 248.3222 ± 1.2073 μg/g, respectively (Supplementary Table S7).

HS induces liver dysfunction and oxidative stress in different recovery stages

High temperature (38 ± 1 °C) and humidity (75 ± 5%) induced a significant elevation of body temperature above 40 °C ($P < 0.001$). After exposure to HS, water consumption and weight loss were much higher ($P < 0.001$, *vs.* control group). At the end of 7 days, the weight gain percentage was significantly lower in the HS group ($P < 0.01$, *vs.* control group) (Fig. S1). Fig. 3A shows the histological changes in the liver following different recovery stage of last heat exposure. The liver parenchyma was damaged in HS rats at different recovery stages. Starting from 3 h after HS, hepatocyte swelling and ballooning degeneration were observed, which indicate an increase in hepatocyte membrane permeability, and necrosis. Meanwhile, we also observed inflammatory infiltration, slight steatosis, and hemorrhage in the central vein expansion and sinusoidal spaces. However, more obvious extensive hepatocyte edemas, ballooning degeneration, and diffuse hemorrhage occurred at 6–12 h after heat exposure (Fig. 3A). Consistent with the changes in liver histopathology, the serum ALT and AST concentrations and the De Ritis ratio (AST/ALT ratio) as measure for liver damage severity were markedly increased as early as 3 h after heat exposure and progressively increased in a time-dependent manner ($P < 0.05$, *vs.* control group) (Fig. 3B). Previous studies have demonstrated that HS can act as a catalyst for oxidative stress in the liver (Liu et al., 2017). To gain more insights into the liver heat-induced oxidative stress, we analyzed several parameters at different time points post heat treatment. Elevated levels of 8-OHDG and MDA ($P < 0.05$, *vs.* control group) were observed at 6–12 h after heat exposure. The CAT level was significantly decreased at 6 h ($P < 0.05$, *vs.* control group). CAT levels also decreased at other recovery time stages after heat exposure, but the difference was not

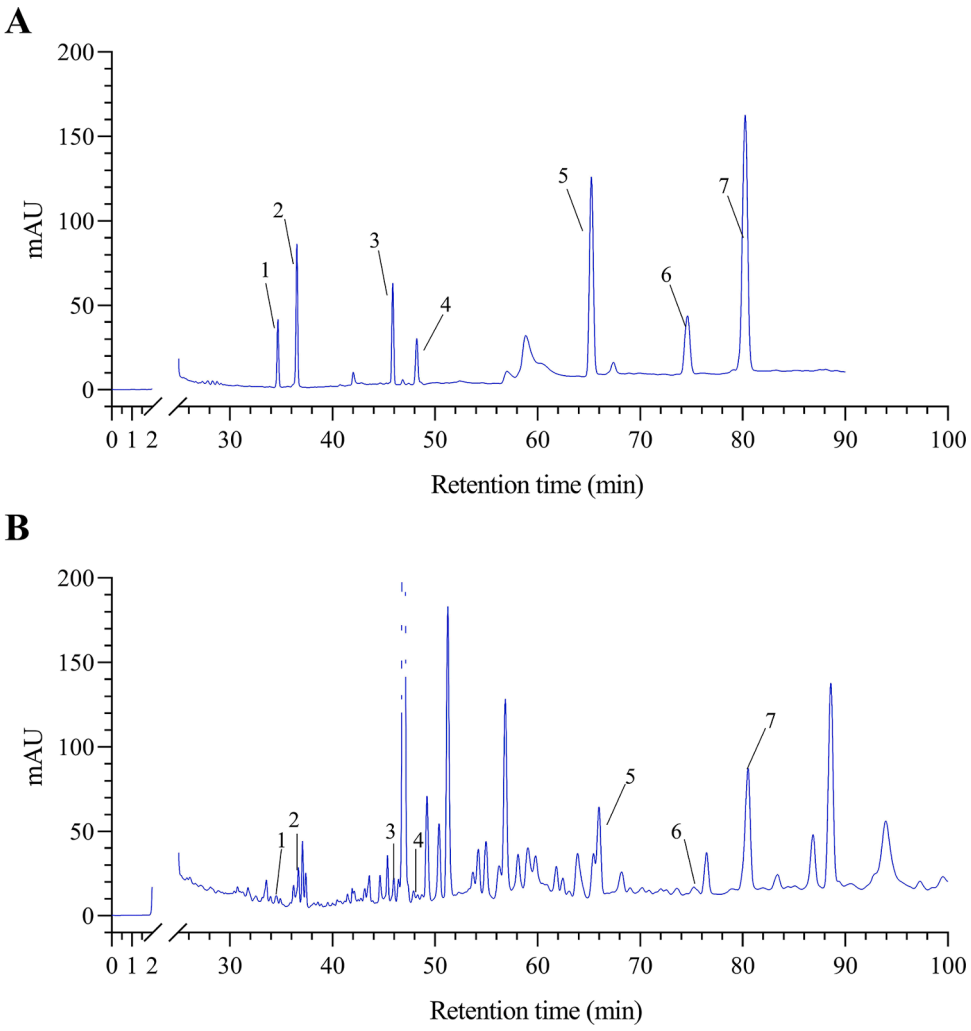

Fig. 2. HPLC chromatogram in SMS. (A) Mixed standards; (B) SMS sample. The identified peaks were listed as follow: 1, ginsenoside Rb1; 2, ginsenoside Rh1; 3, ginsenoside Rg3; 4, ophiopogonin D; 5, ruscogenin; 6, schisandrin A.

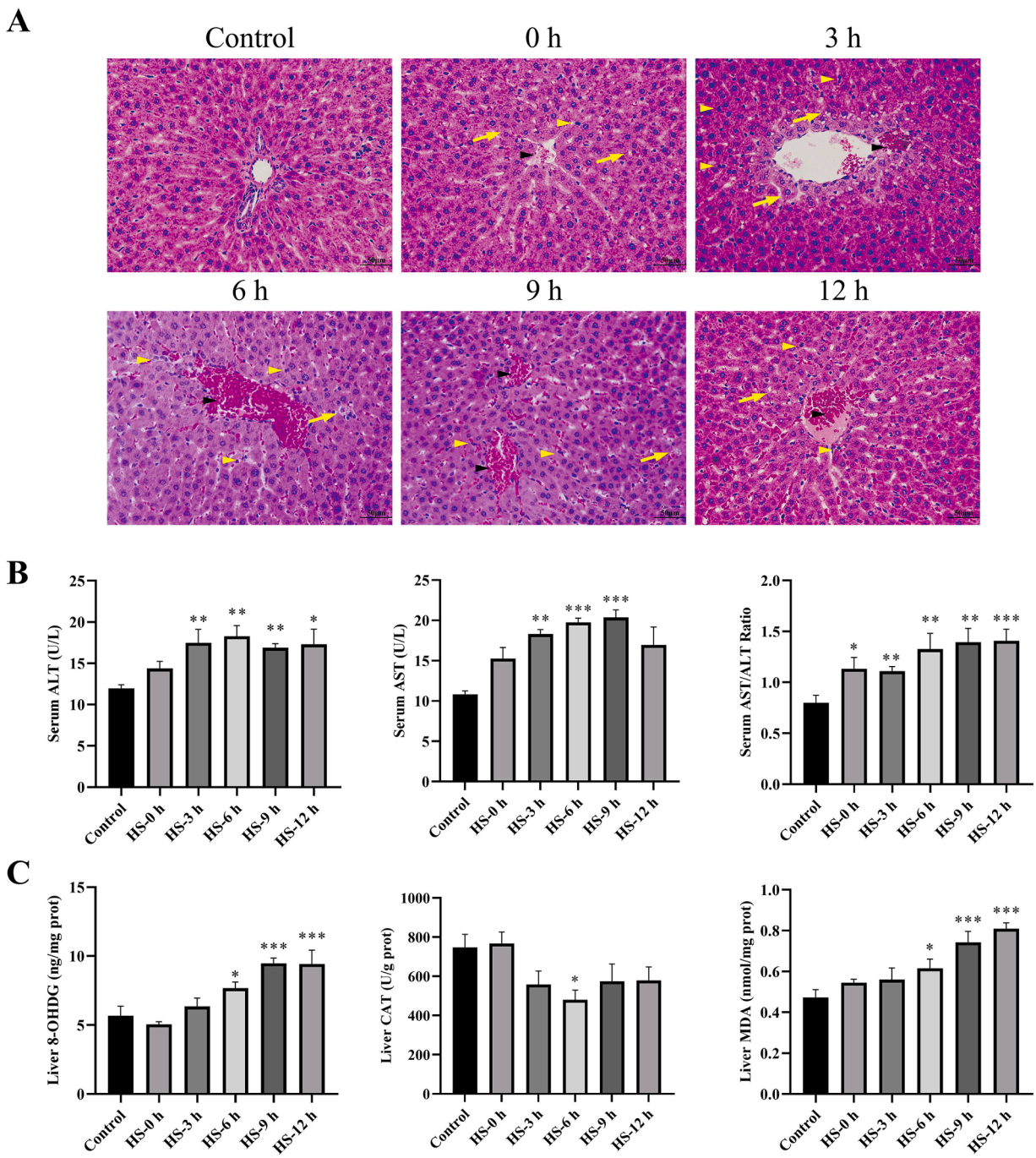

Fig. 3. Heat stress induced liver injury and oxidative stress at different recovery time stages. (A) Histopathology changes in liver at the recovery time point after heat stress (scale bar = 50 μm; 200 × magnification). Black arrowheads point to hemorrhage in the expansion central vein and sinusoidal spaces. Yellow arrowheads point to inflammatory infiltration. Yellow arrows point to ballooning degeneration; (B) ALT, AST levels, and AST/ALT ratio in serum at 0, 3, 6, 9, and 12 h after HS induction; (C) 8-OHDG, CAT, and MDA concentration in liver tissue lysate. Data are expressed as the mean ± SEM, except for histological section analysis $n = 5$ per group, the remaining analysis $n = 8$ per group. $^{*}P < 0.05$, $^{**}P < 0.01$, and $^{***}P < 0.001$ compared with control group.

significant ($P > 0.05$, *vs.* control group) (Fig. 3C).

Taken together, these findings indicated that liver injury and oxidative stress is absent at the onset of HS, but presents during HS recovery time. The 6 h recover time is an important time point after heat exposure. Thus, we chose this time point for follow-up work according to the above results.

SMS alleviates HS-induced injury in rat liver

Before we conducted molecular characterization of the liver, we first measured the basic physiological parameters of rats exposed to HS and SMS-treated. The HS induced rats gradually developed clinical symptoms such as body weight loss. Rectal temperature and water consumption were significantly higher in HS-induced rats than tin the control group ($P < 0.001$) (Fig. 4A, Supplementary Data S1). In addition, the serum ALT, AST, and De Ritis ratio (AST/ALT ratio) of the HS exposed group were significantly increased compared with the control group ($P < 0.001$) (Fig. 4B). The liver injury macroscopic score was significantly higher in the HS-exposed group than in the control group ($P < 0.001$) (Fig. 4C). These results showed that the HS rat model was

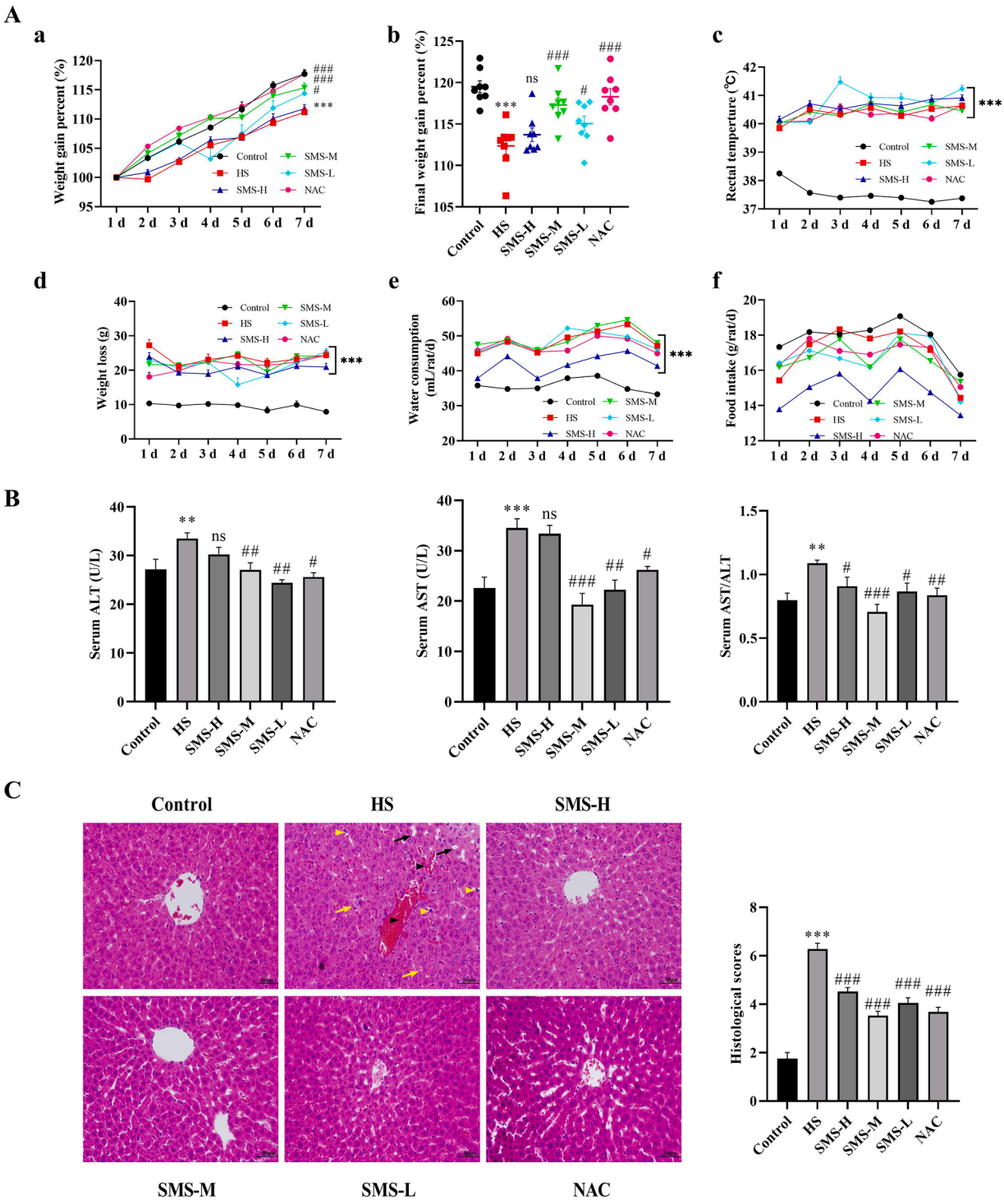

Fig. 4. SMS intervention relieves HS-induced liver injury in rats. (A) Physiological changes of SMS on heat stress rats. (a) body weight gain percent; (b) final weight gain percent; (c) the rectal temperature during pre- and post-heat stress; (d) the weight loss during pre- and post-heat stress; (e) water consumption; (f) food intake. (B) Hepatocellular function evaluated by ALT, AST, and AST/ALT ratio in serum; (C) Representative light microscopy photographs and histological scores of liver injury are shown (scale bar = 50 μm; 200 × magnification). The arrow and arrowheads' meaning were consistent with above. Data are expressed as the mean ± SEM, except for histological scores analysis $n = 5$ per group, the remaining analysis $n = 8$ per group. $^{**}P < 0.01$, $^{***}P < 0.001$ *vs.* control group; $^{\#}P < 0.05$, $^{\#\#}P < 0.01$, $^{\#\#\#}P < 0.001$ *vs.* HS group.

successfully achieved.

Different doses of SMS were given during the trial. The results showed that compared with the HS group, SMS intervention (especially SMS-M) could significantly inhibit body weight reduction ($P < 0.001$); reduce ALT, and AST concentrations and De Ritis ratio (AST/ALT ratio) in serum ($P < 0.001$); and alleviate the liver injury caused by heat exposure ($p < 0.001$). However, the high dose of SMS failed to achieve favorable therapeutic effects. The reason may be caused by the increased gavage volume. Furthermore, body weight loss during pre- and post-HS, rectal temperature, water consumption, and food intake were not significantly different after drug intervention.

Effects of SMS on inflammation response in HS-induced rats

Systemic inflammatory response (SIRS) plays a critical role in cellular injury after heat exposure by activating pathways leading to cellular necrosis and apoptosis (Leon, 2007). In our study, we found that the serum and liver myeloperoxidase (MPO) activity was significantly increased in HS rats compared with the control group, indicating that HS model group rats had abnormal immune function and significant inflammatory reactions. However, the administration of SMS to HS rats significantly decreased the level of MPO ($P < 0.05$) (Fig. 5A and B). The liver IL-1β, IL-6, TNF-α and IL-10 mRNA expression levels were detected using RT-qPCR. The liver IL-1β, IL-6, TNF-α, and IL-10 mRNA levels in the HS model group were noticeably higher ($P < 0.05$) than those in the control groups. These indexes were improved to different degrees in SMS and NAC groups, and near the control group ($P < 0.05$) (Fig. 5C through F). IL-10 is an important anti-inflammatory cytokine in the body, IL-10 mRNA expression was reduced in the SMS-treated group after heat exposure. The result may be closely related to the development of HS according to a previous study (Liu et al., 2011). These results suggest that the anti-inflammatory effect of SMS is partly responsible for the treatment of HS.

SMS attenuates HS-induced oxidative injury and heat shock protein (HSP) expression in the liver of rats

To investigate the impact of SMS on heat-induced oxidative stress in the liver, we measured the levels of SOD, GSH, CAT and MDA. The results showed that the activities of enzymatic antioxidants SOD, GSH, and CAT in liver homogenate of HS model group rats were significantly decreased ($P < 0.001$), and the level of MDA was significantly increased ($P < 0.01$), indicating that the levels of oxidative stress in model group rats were significantly enhanced. Nevertheless, compared with HS group rats, different doses of SMS significantly increased SOD and CAT activities, and GSH content, but reduced the generation of MDA, indicating that SMS could relieve heat-induced oxidative stress in the rat liver ($P < 0.05$) (Fig. 6A through D). Previous studies have confirmed that exogenous HSP can stimulate a pro-inflammatory signal transduction cascade that results in the secretion of proinflammatory cytokines, which in turn damage the cells (Asea et al., 2002). Therefore, we examined the effect of SMS on HSP expression in HS rat livers. The data showed that HSP70, HSP90, HSP27 and HSF-1 mRNA expression was significantly increased in the HS group compared with the control group, while it was significantly restored after the administration of SMS ($P < 0.05$) (Fig. 6E through F). These results indicate that the therapeutic effect of SMS on HS is also derived from its antioxidant effect and HSP regulation capacity.

SMS improves HS induced energy metabolism disorder in the liver

Modern medical studies have proposed that energy metabolism disorder plays a crucial role in the development of HS induced organ injuries. Furthermore, energy metabolism disorder has a close relationship with SIRS (Laitano et al., 2020). Nevertheless, few studies have investigated the relationship of energy metabolism with HS-induced liver injury. Therefore, in our study, targeted energy metabolomics and verification analysis were utilized to explore the influence of heat exposure induced liver injury and to evaluate the therapeutic effect of SMS.

Targeted metabolic method validation

To identify whether the established method is suitable for metabolomics analysis, method validation was performed using 40 identified

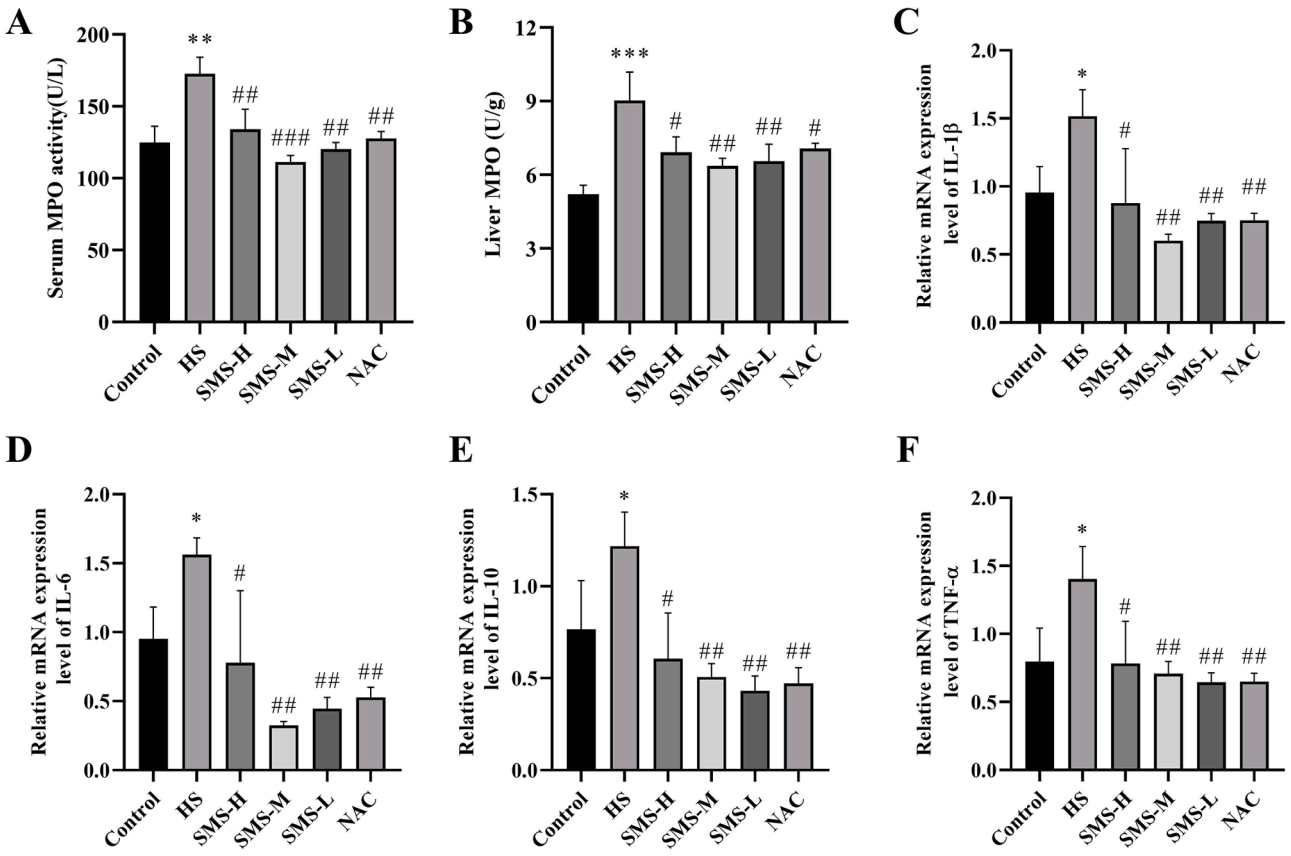

Fig. 5. Treatment by SMS ameliorates HS induced liver inflammation. (A), (B) MPO activity in serum and liver; (C), (F) The inflammation cytokine mRNA expression in liver were detected, including IL-1β (C), IL-6 (D), IL-10 (E), and TNF-α (F). Data are expressed as the mean ± SEM, except for MPO activity analysis $n = 8$ per group, the remaining analysis $n = 5$ per group. $^{*}P < 0.05$, $^{**}P < 0.01$, $^{***}P < 0.001$ *vs.* control group; $^{\#}P < 0.05$, $^{\#\#}P < 0.01$, $^{\#\#\#}P < 0.001$ *vs.* HS group.

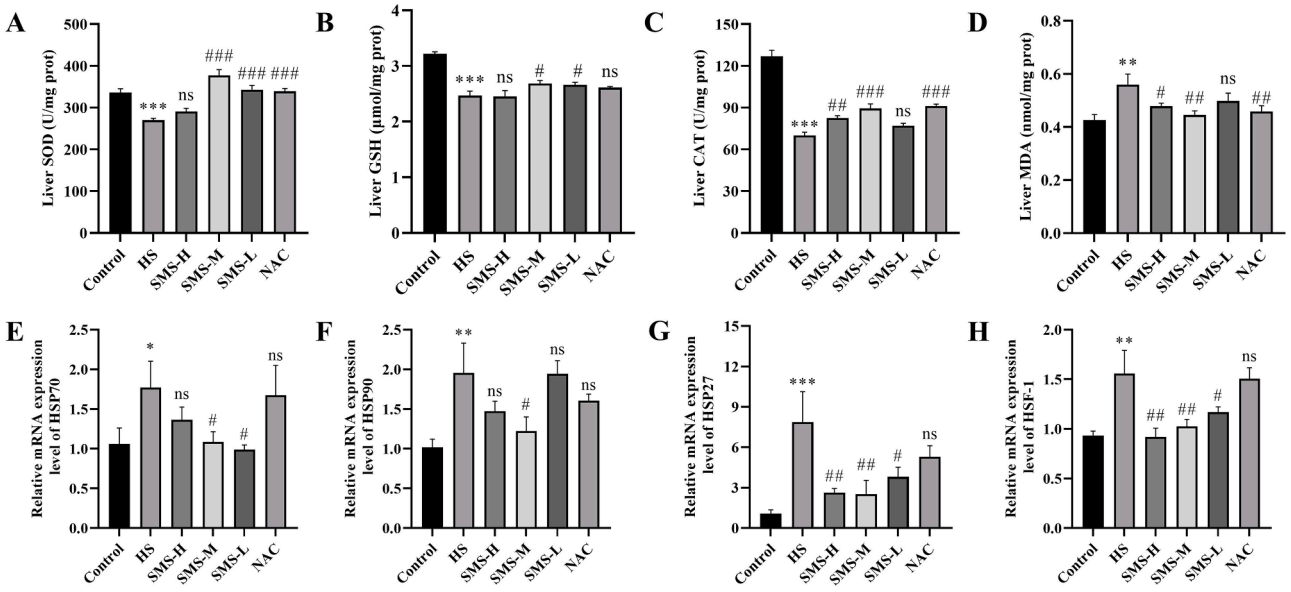

Fig. 6. Effects of SMS on the oxidative stress and heat shock protein mRNA expression of liver in HS-induced rats. (A), (D) Oxidative stress parameters were detected in liver, including SOD (A), GSH (B), CAT (C), and MDA (D). (E), (H) mRNA expression levels of the heat shock protein assessed by RT-qPCR, including HSP70 (E), HSP90 (F), HSP27 (G), and HSF-1 (H). Data are expressed as the mean ± SEM, except for oxidative stress parameters analysis $n = 8$ per group, the remaining analysis $n = 5$ per group. $^{*}P < 0.05$, $^{**}P < 0.01$, $^{***}P < 0.001$ *vs.* control group; $^{\#}P < 0.05$, $^{\#\#}P < 0.01$, $^{\#\#\#}P < 0.001$ *vs.* HS group.

metabolite candicate' ions of chromatographic peak in this study (Fig. S2A). The relative standard deviation of these components across QC samples ranged from 0.46% to 23.31% (Fig. S2B). Two-dimensional PCA scores plot and proportion of variance for analyzed QC samples are presented in the Supplementary Fig. S2C and Table S8. The result of multivariate analysis of QC samples showed that the deviation of the analytical system was acceptable.

Identification of different energy metabolites in liver metabolic profiling

Targeted metabolic analysis was performed to identify energy metabolic alterations, which may provide useful information to elucidate the mechanism of action of SMS. The SMS-M group in which rats were treated with 2.52 g/kg of SMS, was selected to simplify data processing. PCA was performed to visualize and differentiate the sample clustering, trends, and outliers among observations. Metabolic phenotype separations were observed between control *vs.* HS, HS *vs.* SMS, and HS *vs.* NAC groups. The PCA score plots showed that the samples from the control group could be distinctly discriminated from the HS group, which indicated that the normal metabolic profile of rats was disturbed owing to heat exposure, whereas the samples of the SMS and NAC groups were obviously divided from the HS group, which presented good quality parameters (Fig. 7A, Supplementary Fig. S3 and Table S8). To visualize the intensity of each metabolite, hierarchical cluster analysis (HCA) heatmap was performed, where each colored cell on the map corresponds to a concentration value of metabolite. Samples from different groups displayed different color distributions, even though the eight biological replicates of each group exhibited similar color layouts (Fig. 7B). To sum up, the results of multivariate statistical analysis of PCA and HCA were highly coincident. *Student's t-test* was used to determine the variations of these metabolites between groups. The actual fold changes of all metabolite species ($P < 0.05$) are shown in Fig. 7D, Supplementary Table S9 and Data S2.The liver levels of 16 energy metabolites, such as fructose 6-phosphate, pyruvate and acetyl-CoA, were significantly changed in HS group compared with the control group ($P < 0.05$). However, these changes were partly regulated after SMS and NAC treatment. Interestingly, the intensity of several metabolites, such as citrate and cis-aconitate, was not reversed. Meanwhile, some metabolites, including isocitrate, succinate, and fructose 6-phosphate, were significantly increased in SMS-treated HS-induced rats ($P < 0.05$). Nevertheless, no significant change was observed in the HS group compared with the control group ($P > 0.05$). The regulations on the TCA cycle and glycolysis were possibly related to the protective effects of SMS on HS-induced liver energy disorder. Notably, compared with the control group, the HS group had significantly lower ratios of AMP/ATP and ADP/ATP (AMP/ATP or ADP/ATP, an indicator of AMPK activity). However, the change was found to reverse to the tendency of the control group after SMS and NAC treatment (Fig. 7D and Supplementary Table S9 and Data S2).

SMS regulates the mRNA expression of energy-related genes and glycogen content in HS-induced liver injury

The metabolomic study demonstrated that SMS intervened in the TCA cycle and glycolysis caused by HS induced liver energy disorder, which may be mediated by regulating the rate-limiting enzymes in these metabolic pathways. Thus, to verify our hypothesis, the expression of rate-limiting enzymes was quantitatively evaluated to investigate the therapeutic effect of SMS on HS-induced energy disorder in the liver using RT-qPCR. The expression levels of Pklr and Pgk1, key enzymes in glycolysis, were significantly decreased in the HS group compared with the control group ($P < 0.05$), but the expression levels of Pfk1 and Gck were not significantly changed ($P > 0.05$). Nevertheless, the four key enzymes had significantly higher levels after SMS or NAC treatment. In the TCA cycle, the mRNA expression level of Sdhb was obviously decreased in the HS group. The expression levels of other enzymes including Cs, Idh3a, Ogdh, Fh, and Mdh2 were not significantly different between the control and HS groups ($P > 0.05$), but changed significantly after drug intervention ($P < 0.05$). Under anaerobic condition, lactate is generated from pyruvate by the action of LDH. We found that SMS could attenuate Ldha mRNA expression caused by HS-induced anaerobic respiration in the liver ($P < 0.05$) (Fig. 7C). Furthermore, we detected the glycogen storage function by PAS staining. Compared with the control group, the glycogen content in the HS group was significantly reduced, which could be significantly inhibited by SMS treatment (Fig. 7E).

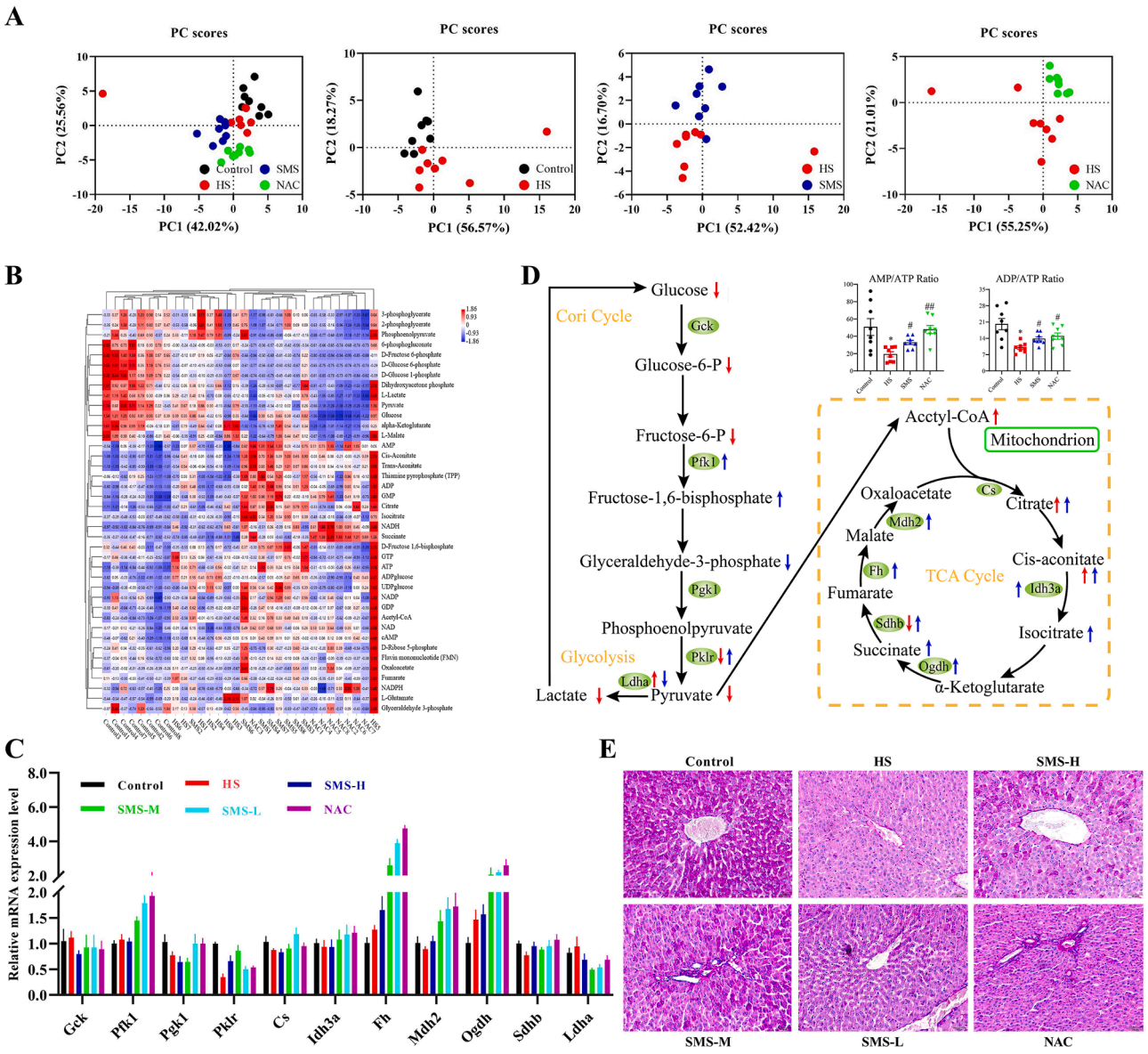

Fig. 7. Energy metabolism plays a central role in heat stress induced liver injury. (A) The PCA score plots of energy metabolites in four groups (Control, HS, SMS-M and NAC groups) based on UPLC–MS/MS–MRM. (B) Hierarchical cluster analysis (HCA) of energy metabolites in different groups, respectively. The heatmap presents relative abundance of the metabolites with different colors, where deeper red represents higher intensity and deeper blue represents lower intensity. (C) mRNA relative expression of six groups related to energy metabolism in rat livers. (D) The regulation of SMS on energy metabolic disorders caused by heat stress in liver. Compared with control group the alterations in metabolites in HS group are labeled with a red arrow and the changes in SMS group compared with HS group are labeled with blue. The upward arrow indicates a significant increase ($P < 0.05$) and the downward arrow indicates a significant decrease ($P < 0.05$). (E) PAS (periodic acid-Schiff) stain using formalin-fixed, paraffin-embedded slides (scale bar = 50 μm;200 × magnification). Data are expressed as the mean ± SEM, except for UPLC–MS/MS–MRM analysis $n = 8$ per group, the remaining analysis $n = 5$ per group. $^{*}P < 0.05$, $^{**}P < 0.01$, $^{***}P < 0.001$ *vs.* control group; $^{\#}P < 0.05$, $^{\#\#}P < 0.01$, $^{\#\#\#}P < 0.001$ *vs.* HS group.

SMS ameliorates HS-induced liver mitochondrial damage via an AMPK-mediated drp1-dependent autophagy process

Given that mitochondria are a target for cellular stress, we examined whether SMS could protect mitochondrial morphology and function. Fig. 8A shows the changes in liver tissue ultrastructure, which shows distortion in cellular organelles such as mitochondria and nucleus. Nuclear membrane deformation, chromatin aggregation, distortion in shape along with mitochondrial swelling, and autophagy were observed in the HS group compared with the control group (Fig. 8A a,b). However, the damages in ultrastructural orientation, nuclear membrane, and mitochondrial shape were ameliorated in SMS- or NAC-treated group compared with the HS group (Fig. 8A c,d). Heat exposure induces cytochrome c (Cytc) release into the cytosol from mitochondria. Thus, the Cytc level in the cytosol can be used to evaluate the extent of mitochondrial damage. As we expected, SMS inhibited HS-induced mitochondrial release of Cytc ($P < 0.05$) (Fig. 8B). The results indicate that SMS could restore the mitochondrial damage and prevent Cytc release to the cytosol.

From the targeted metabolomic results, the most prominent metabolic alteration was the AMP/ATP and ADP/ATP ratios. AMPK serves as a central mediator of cellular response to energetic stress and mitochondrial insults. Several studies have confirmed that AMPK is activated by increases in AMP/ATP and ADP/ATP ratios (Garcia and Shaw, 2017). Thus, we presumed that SMS treatment might activate AMPK to promote the recovery of liver mitochondria from HS-induced damage. We

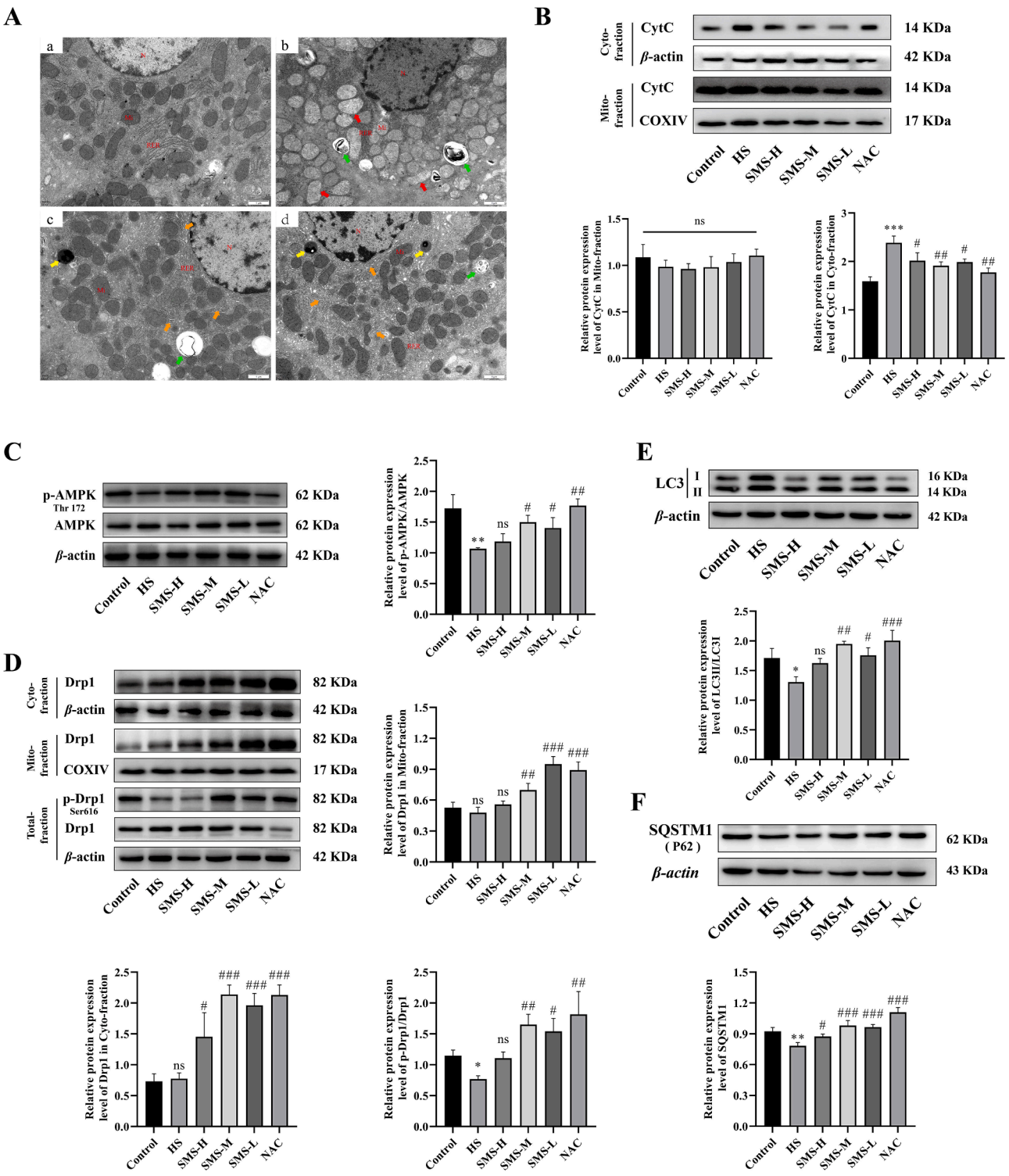

Fig. 8. SMS ameliorates heat stress induced mitochondrial dysfunction through the activation of AMPK-mediated Drp1-dependent autophagy in rat livers. (A) Representative liver ultrastructural features in Control (a), HS (b), SMS (c), and NAC groups (d). The red arrows point to swollen mitochondria. The green arrows point to autophagosomes. The yellow arrows point to secondary lysosomes. The orange arrows point to slightly expanded rough surfaced endoplasmic reticulum. N: nucleus; Mi: mitochondria; RER: rough surfaced endoplasmic reticulum. (scale bar = 1 μm; 15,000 × magnification). The protein expression levels of Cytc (B), p-AMPKα^{Thr172} and AMPKα (C), Drp1^{Ser616} and Drp1 (D), LC3B (E), and SQSTM1/ p62 (F) were detected by western blotting in liver tissues. β-Actin served as a loading control protein for whole level and cytosolic fraction and COXIV as internal reference protein for mitochondrial fraction. Data are expressed as the mean ± SEM, except for the ultrastructural analysis $n = 3$ per group, the remaining analysis $n = 5$ per group. $^{*}P < 0.05$, $^{**}P < 0.01$, $^{***}P < 0.001$ *vs.* control group; $^{\#}P < 0.05$, $^{\#\#}P < 0.01$, $^{\#\#\#}P < 0.001$ *vs.* HS group.

observed that phosphorylated AMPKα^{Thr172} levels in the livers of rats were decreased after HS ($P < 0.05$), which was consistent with previous studies on HS-induced liver damage. However, compared with the HS group, the SMS and NAC group exhibited significantly higher hepatic p-AMPKα^{Thr172} levels ($P < 0.05$) (Fig. 8C).

Drp1, a member of the dynamin family, is a key player in mitochondrial fission and mitophagy (Chen et al., 2021). Recently, several lines of evidence indicate that AMPK promotes mitophagy through the phosphorylation of Drp1-mediated mitochondrial fission (Wang and Youle, 2016). Therefore, we assessed mitochondrial fission protein Drp1. The cytosolic and mitochondrial Drp1 levels were upregulated after heat exposure and were markedly higher in the SMS or NAC group compared with the HS group. Meanwhile, HS significantly inhibited the phosphorylation of Drp1^{Ser616} in liver tissues ($P < 0.05$). Nevertheless, SMS and NAC significantly increased p-Drp1^{Ser616} activity in the livers of HS-induced rats ($P < 0.05$) (Fig. 8D). To investigate whether SMS promotes autophagy in the liver of rats after HS, we examined the protein levels of two markers of autophagy, LC3B-II/LC3B-I and SQSTM1/p62. We found that SMS significantly increased LC3B-II/LC3B-I protein expression level in HS-induced rat livers compared with the HS group (Fig. 8E). Additionally, SQSTM1/p62 protein expression was significantly increased following SMS or NAC treatment ($P < 0.05$) (Fig. 8F). Taken together, these results showed that SMS could phosphorylate AMPKα^{Thr172} in HS-induced rat livers, which coordinates mitochondrial fission and mitophagy in the response to mitochondrial insults.

Discussion

The liver is one of the most sensitive organs in hot environment. HS leads to severe damage to the liver, which is validated by liver dysfunction, oxidative stress, inflammatory response and distortion in hepatic parenchyma (Davis et al., 2017; Kew et al., 1970). At present, due to HS is becoming an increasing morbidity and mortality burden, no safe and effective therapies for HS are available in clinics. SMS has attracted considerable attention due to its natural antioxidant and anti-inflammation capacity in HS-induced animal models and patients. Nevertheless, the mechanisms underlying the hepatoprotective property of SMS on HS-induced rats remains unclear. In the present study, we systematically evaluated the therapeutic effect of SMS on HS-induced rats from the point view of liver function, histopathologic changes, oxidative stress and inflammation. Moreover, on the basis of targeted metabolomics, we have demonstrated that SMS affords protection on HS-induced liver insults and that an AMPK-mediated autophagy process plays a crucial role via regulating Drp1-dependent mitochondrial fission and energy metabolism disorder (Fig. 9).

Previous studies have indicated that liver injury is absent at the initial stage of HS, but appears during HS recovery in clinical cases and animal models (Davis et al., 2017; Geng et al., 2015). Accumulating evidence have well confirmed that liver damage is may be a consequence of the oxidative injury-mediated inflammation response that ensues during the later period of HS (Du et al., 2021). Consistent with previous reports, this study showed that heat exposure triggered a series of more severe damage features in the liver at 6 h via the evaluation of serum enzyme (ALT, AST, and AST/ALT ratio) and oxidative stress (8-OHDG, CAT, and MDA) indicators. Hence, the inhibition of oxidative stress and inflammatory response plays a pivotal role in the treatment of HS-induced liver insult during recovery. Accumulating evidence have demonstrated that SMS and its natural compounds could elevate

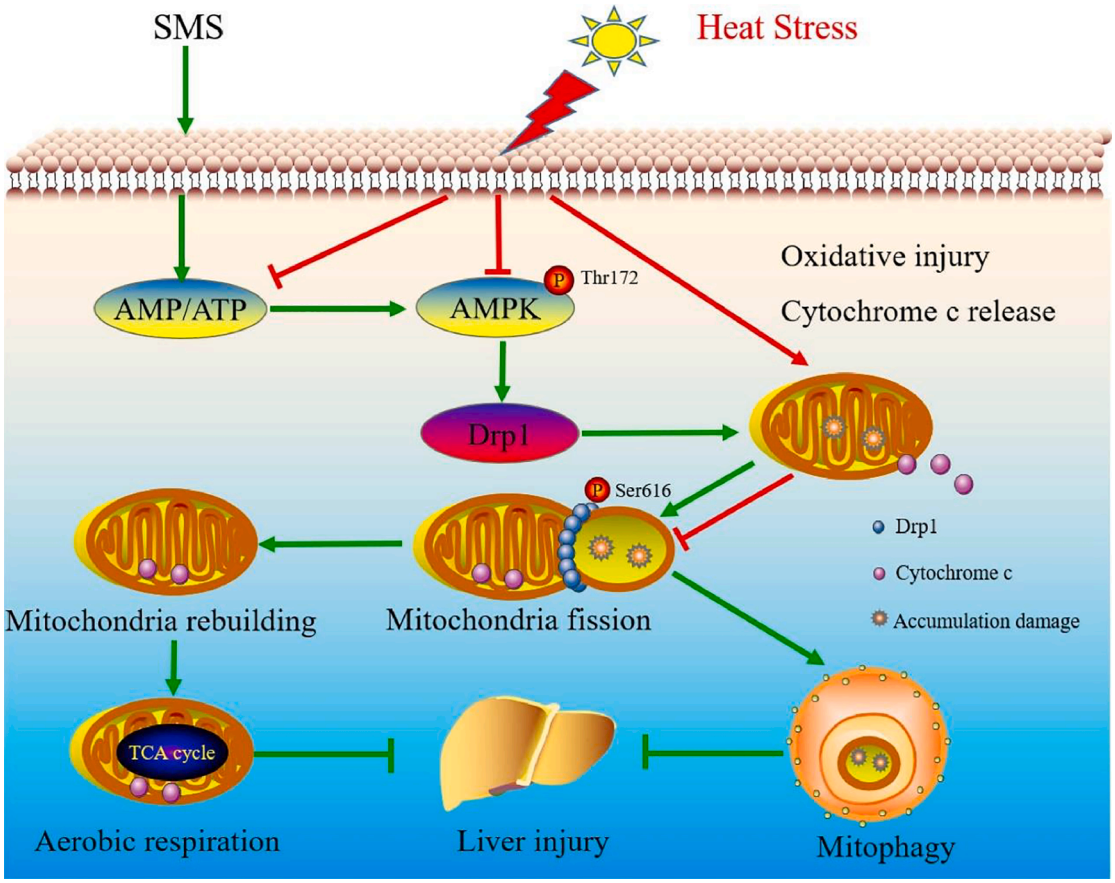

Fig. 9. Schematic diagram of the mechanism of SMS protecting rats from HS-induced liver injury. In hepatocytes, heat stress leads to mitochondrial damage induced oxidative injury and cytochrome c release to cytosolic. SMS could attenuate the oxidative injury in HS-induced rat livers through AMPK-mediated Drp1-dependent mitophagy and mitochondria rebuilding.

thermotolerance, inhibit inflammatory response and maintain redox balance during heat stroke in rats (Wang et al., 2005a, 2005b). Our pharmacological investigation showed that SMS could improve liver dysfunction and protect against HS-induced hepatic cell damage. SIRS plays a critical role in cellular injury after heat exposure by activating inflammatory pathways leading to cellular necrosis and apoptosis (Leon, 2007). MPO, an abundant hemoprotein present in neutrophils and monocytes, is often used to evaluate the degree of inflammatory response in organisms. In our study, we found that SMS attenuated the activity of MPO in serum and liver tissue. Meanwhile, the expression of inflammatory cytokines, including IL-1β, TNF-α, IL-6, and IL-10, was decreased. Strangely, the anti-inflammatory cytokine IL-10 was decreased after SMS treatment, which may be attributed to the developmental period of HS-induced SIRS according to early studies (Leon et al., 2006; Liu et al., 2011). However, the underlying mechanisms need to be explored in the future. SOD, CAT, and GSH are the major antioxidant substances for controlling reactive oxygen, and MDA is the most abundant product in the process of lipid peroxidation (Slimen et al., 2014). As we expected, SMS could upregulate SOD and CAT activities and GSH content, and inhibit the production of MDA on HS-induced liver oxidative injury. All pro-inflammatory cytokines and abrupt production of free radicals contribute to mitochondrial dysfunction (Slimen et al., 2014). We also observed swelling mitochondria and disrupted crista in HS-induced rat liver by TEM analysis, but SMS treatment reversed these effects. Furthermore, we confirmed that HS obviously upregulated the mRNA expression of HSPs and HSF-1in rat liver. The activation of heat shock transcription factors is vital to heat shock response, leading to the production of HSPs. As ubiquitous molecular chaperones, HSPs can maintain protein homeostasis and attenuate inflammatory exudation against organ damage and lethality under stressful conditions (Leon, 2007). Nevertheless, overexpressed HSPs can be released from the cytoplasm into the extracellular space, which in turn promotes the secretion of proinflammatory cytokines by binding to various receptors (Asea et al., 2002; Zhang et al., 2020). Therefore, appropriate levels of HSPs in the body need to be sustained. In our study, we found high mRNA expression of HSPs, such as HSP70, HSP90, HSP27 and HSF-1, in liver tissue of rats exposed to HS, but SMS intervention can restore and maintain HSP homeostasis to counter HS-induced damage. In short, although our results provided further evidences that SMS can ameliorate liver dysfunction, inflammatory response and pathological damage through regulating the antioxidative system and HSP homeostasis, how SMS exerts its therapeutic effects remains unclear.

The metabolic alteration of the liver is important for the successful adjustment of the physiological and biochemical pathways to any adverse environmental stressors. The liver is a central organ coordinating lipid, carbohydrate, and protein metabolism (Ippolito et al., 2014). Numerous pieces of evidence suggest that HS leads to severe energy crisis and oxidative stress, which give rise to downregulated oxidative phosphorylation and TCA cycle (Laitano et al., 2020). Thus, in our study, we explored that the relationship between SMS therapy and energy metabolism disorder on HS rat livers through targeted energy metabolomics technique. Prolonged exposure to high ambient temperature increases oxygen consumption and reduces splanchnic circulation, resulting in hypoxia in visceral organs and leading to the upregulation of anaerobic glycolysis (Slimen et al., 2014). Our data presented that glucose, glucose-6-P and fructose-6-P were decreased, indicating insufficient source of fuel for energy supply, resulting in negative energy balance in HS-induced rat livers. Fructose-1,6-bisphosphae is generated from fructose-6-P by the action of a rate-limiting enzyme Pfk1 during glycolysis. We found that the mRNA expression of Pfk1 was increased after SMS treatment in HS-induced rat liver, which is consistent with the elevation of fructose-1,6-bisphosphae. Pklr catalyzes the conversion of phosphoenolpyruvate to pyruvate, which converts to acetyl coenzyme A to pass into the TCA cycle under aerobic conditions, while it converted to lactate by activating LDH under anaerobic conditions (Zhu et al., 2020). In our study, HS leads to decreased gene expression of Pklr in rat liver, but SMS could up-regulate it, which may facilitate the production of pyruvate to participate in energy metabolism. We observed that SMS inhibits the high expression of Ldha in HS-induced rat liver to attenuate oxidative injury due to hypoxia. Interestingly, the lactate content was not increased in rat liver after heat exposure, which may be associated with the Cori cycle to create glucose in the liver. Oxygen deficiency and oxidative stress can damage mitochondria and inhibit the activity of TCA cycle enzymes, leading to energy metabolism disorder (Laitano et al., 2020). Our metabolomic results revealed marked changes in the concentration of some TCA cycle intermediates, namely citrate, cis-aconitate, isocitrate and succinate after SMS treatment in HS-induced rat liver. Similarly, high expression of related genes (Idh3a, Ogdh, Sdhb and Mdh2) in the TCA cycle was observed. SDH is located in the inner mitochondrial membrane and catalyzes the conversion of succinate to fumarate (Edalat et al., 2015). We observed that the expression of Sdha in rat liver was decreased after heat exposure, indicating mitochondrial dysfunction and an energy crisis, while SMS could reverse this effect. Thus, mitochondrial homeostasis might play a role in relieving HS, thereby contributing to the maintenance of energy demand.

AMPK, a highly conserved serine/threonine kinase, is activated in response to energy stress by sensing increases in AMP/ATP and ADP/ATP ratios to promote ATP generation and energy restoration and maintain cellular energy homeostasis (Garcia and Shaw, 2017). Previous studies demonstrated that AMPK phosphorylation is downregulated *in vitro* and *in vivo* HS models (Tsai et al., 2016; Xia et al., 2019). Intriguingly, we found that AMP/ATP and ADP/ATP ratio were elevated after SMS intervention in HS-induced rat liver. Meanwhile, we observed that SMS can facilitate the phosphorylation of AMPK at Thr172 site. HS induces severe oxidative stress, which is apparent throughout the recovery period, causing mitochondrial dysfunction and mitophagy imbalance (Laitano et al., 2020). In our study, the expression of Cytc was significantly elevated in the cytosol, which indicates that HS induced mitochondrial dysfunction. AMPK is a crucial and direct regulator of mitochondrial dynamics (Herzig and Shaw, 2018). Mitochondria are highly mobile organelles that constantly undergo fusion and division to generate a dynamic and interconnected network. Drp1 is a key player in mitochondrial fission. The activation of AMPK results in increased localization of Drp1 in mitochondria (Wang and Youle, 2016). Our data showed that SMS activated phosphorylation at Ser616 of Drp1, leading to Drp1 translocation into the outer mitochondria membrane to induce mitochondrial fission. Recent reports demonstrated that a Drp1-dependent autophagy process facilitates the rebuilding of the mitochondrial network and modulates adaptation capacity in response to acute HS (Chen et al., 2021). The cleavage of LC3-I to form LC3-II is indicative of autophagy occurrence. We observed that the LC3B-II/LC3B-I ratio was upregulated after SMS treatment in HS-induced rat livers. As a selective autophagic receptor, p62 can connect LC3, and then be integrated into autophagy and degraded in autophagy lysosomes (Pankiv et al., 2007). However, our study showed that SMS promoted autophagy flux and upregulated p62. Recent works presented that SQSTM1/p62 plays an important role in ameliorating the deleterious effects of HS. The overexpression of a selective autophagy receptor is sufficient to induce autophagy and enhance longevity and protein stability (Kumsta et al., 2019). These results confirmed that the therapeutic effects of SMS were attributed to the regulation of energy metabolism and AMPK/Drp1-dependent mitophagy process. Although our results preliminarily demonstrated that SMS plays a key role in maintaining mitochondrial homeostasis for attenuating HS-induced liver insults, the key indicators of mitochondrial function need to be further evaluated through *in vitro* models in the future. Furthermore, how Drp1 mediates autophagy to facilitate mitochondrial rebuilding needs to be elucidated.

Conclusions

In conclusion, using a HS-induced rat liver injury model, we systematically evaluated the therapeutic effects of SMS in the liver on the basis of physiological-biochemical indices, histomorphology, and furthermore combined with targeted energy metabolomics and molecular biology verification. Our work indicated that SMS attenuates HS-induced liver damage through regulating liver function, restoring histological injury, altering abnormal energy metabolism, and sustaining mitochondria structure and function homeostasis. Notably, we have preliminarily proved that the protective mechanisms of SMS are attributed to an AMPK-mediated Drp1-dependent mitophagy and mitochondria rebuilding process, which in turn alleviate HS-mediated rat liver damage and energy expenditure. Targeting AMPK, mitochondrial fission, and mitophagy may serve as effective approaches to inhibit the HS-induced liver injury, and our study lends further support to the use of SMS in treating HS condition.

CRediT authorship contribution statement

X.S. Z. and Y.M. W. conceived and designed the experiments. X.S. Z. and Y.Z. W. analyzed and interpreted the data. X.S. Z. wrote the manuscript. X.S. Z., Y.Q. J. and J.M. R. performed the experiments. Y.Q. W. and Y.H. Z. performed tissue sample collection. X.S. Z. performed pathological sections. P. Ji., W.L. Y. and Y.L. H. read and revised the manuscript. All data were generated in-house, and no paper mill was used. All authors agree to be accountable for all aspects of work ensuring integrity and accuracy.

CRediT authorship contribution statement

Xiaosong Zhang: Conceptualization, Visualization, Formal analysis, Data curation, Writing – original draft, Investigation. **Yaqian Jia:** . **Ziwen Yuan:** . **Yanqiao Wen:** Conceptualization. **Yahui Zhang:** Formal analysis, Data curation, Conceptualization. **Jianmin Ren:** Visualization. **Peng Ji:** Writing – review & editing. **Wanling Yao:** Writing – review & editing. **Yongli Hua:** Writing – review & editing. **Yanming Wei:** Conceptualization, Visualization.

Declaration of Competing Interest

The authors have no conflicts of interest to declare.

Acknowledgments

This study was supported by the National Natural Science Foundation of China (No. 32060812), Industrial R&D Support Project in High Education of Gansu Province (2020C-14), and China Agriculture Research System of MOF and MARA (CARS-37). We are grateful to all other staff in the Institute of Traditional Chinese Veterinary Medicine of Gansu Agricultural University for their assistance in the experiments. We also would like to thank the Shanghai Bioprofile Technology Company Ltd. for providing us with UPLC-MS/MS analysis.

Supplementary materials

Supplementary material associated with this article can be found, in the online version, at doi:10.1016/j.phymed.2021.153920.

References

Asea, A., Rehli, M., Kabingu, E., Boch, J.A., Bare, O., Auron, P.E., Stevenson, M.A., Calderwood, S.K., 2002. Novel signal transduction pathway utilized by extracellular HSP70: role of toll-like receptor (TLR) 2 and TLR4. J. Biol. Chem. 277, 15028–15034. https://doi.org/10.1074/jbc.M200497200.

Bouchama, A., Knochel, J.P., 2002. Heat stroke. New Engl. J. Med. 346, 1978–1988. https://doi.org/10.1056/NEJMra011089.

Chen, S.L., Liu, A., Li, Q., Toru, S., Zhu, G.W., Sun, Y., Dai, Y.T., Zhang, J., Zhang, T.J., Takehisa, T., Liu, C.X., 2016. Research strategies in standard decoction of medicinal slices. China J. Chin. Mater. Med. 41, 1367–1375. https://doi.org/10.4268/cjcmm20160801.

Chen, Y., Leboutet, R., Largeau, C., Zentout, S., Lefebvre, C., Delahodde, A., Culetto, E., Legouis, R., 2021. Autophagy facilitates mitochondrial rebuilding after acute heat stress via a DRP-1-dependent process. J. Cell Biol. 220 https://doi.org/10.1083/jcb.201909139.

Davis, B.C., Tillman, H., Chung, R.T., Stravitz, R.T., Reddy, R., Fontana, R.J., McGuire, B., Davern, T., Lee, W.M., Acute Liver Failure Study, G., 2017. Heat stroke leading to acute liver injury & failure: a case series from the acute liver failure study group. Liver Int. 37, 509–513. https://doi.org/10.1111/liv.13373.

Du, D., Lv, W., Su, R., Yu, C., Jing, X., Bai, N., Hasi, S., 2021. Hydrolyzed camel whey protein alleviated heat stress-induced hepatocyte damage by activated Nrf2/HO-1 signaling pathway and inhibited NF-kappaB/NLRP3 axis. Cell Stress Chaperones 26, 387–401. https://doi.org/10.1007/s12192-020-01184-z.

Edalat, A., Schulte-Mecklenbeck, P., Bauer, C., Undank, S., Krippeit-Drews, P., Drews, G., Dufer, M., 2015. Mitochondrial succinate dehydrogenase is involved in stimulus-secretion coupling and endogenous ROS formation in murine beta cells. Diabetologia 58, 1532–1541. https://doi.org/10.1007/s00125-015-3577-9.

Fu, D.A., Campbell-Thompson, M., 2017. Periodic Acid-Schiff staining with diastase. Methods Mol. Biol. 1639, 145–149. https://doi.org/10.1007/978-1-4939-7163-3_14.

Garcia, D., Shaw, R.J., 2017. AMPK: mechanisms of cellular energy sensing and restoration of metabolic balance. Mol. Cell 66, 789–800. https://doi.org/10.1016/j.molcel.2017.05.032.

Geng, Y., Ma, Q., Liu, Y.N., Peng, N., Yuan, F.F., Li, X.G., Li, M., Wu, Y.S., Li, B.L., Song, W.B., Zhu, W., Xu, W.W., Fan, J., Su, L., 2015. Heatstroke induces liver injury via IL-1beta and HMGB1-induced pyroptosis. J. Hepatol. 63, 622–633. https://doi.org/10.1016/j.jhep.2015.04.010.

Gonzalez-Rivas, P.A., Chauhan, S.S., Ha, M., Fegan, N., Dunshea, F.R., Warner, R.D., 2020. Effects of heat stress on animal physiology, metabolism, and meat quality: a review. Meat Sci. 162, 108025 https://doi.org/10.1016/j.meatsci.2019.108025.

Gupta, A., Sharma, D., Gupta, H., Singh, A., Chowdhury, D., Meena, R.C., Ganju, L., Kumar, B., 2021. Heat precondition is a potential strategy to combat hepatic injury triggered by severe heat stress. Life Sci. 269, 119094 https://doi.org/10.1016/j.lfs.2021.119094.

Heijnen, B.H., Straatsburg, I.H., Gouma, D.J., van Gulik, T.M., 2003. Decrease in core liver temperature with 10 °C by *in situ* hypothermic perfusion under total hepatic vascular exclusion reduces liver ischemia and reperfusion injury during partial hepatectomy in pigs. Surgery 134, 806–817. https://doi.org/10.1016/s0039-6060(03)00125-9.

Herzig, S., Shaw, R.J., 2018. AMPK: guardian of metabolism and mitochondrial homeostasis. Nat. Rev. Mol. Cell Bio 19, 121–135. https://doi.org/10.1038/nrm.2017.95.

Hu, J.M., Hsu, C.H., Lin, Y.C., Kung, C.W., Chen, S.Y., Lin, W.T., Cheng, P.Y., Shen, H.H., Lee, Y.M., 2021. Ethyl pyruvate ameliorates heat stroke-induced multiple organ dysfunction and inflammatory responses by induction of stress proteins and activation of autophagy in rats. Int. J. Hyperth. 38, 862–874. https://doi.org/10.1080/02656736.2021.1931479.

Ippolito, D.L., Lewis, J.A., Yu, C., Leon, L.R., Stallings, J.D., 2014. Alteration in circulating metabolites during and after heat stress in the conscious rat: potential biomarkers of exposure and organ-specific injury. BMC Physiol. 14, 14. https://doi.org/10.1186/s12899-014-0014-0.

Kew, M., Bersohn, I., Seftel, H., Kent, G., 1970. Liver damage in heatstroke. Am. J. Med. 49, 192–202. https://doi.org/10.1016/s0002-9343(70)80075-4.

Kumsta, C., Chang, J.T., Lee, R., Tan, E.P., Yang, Y., Loureiro, R., Choy, E.H., Lim, S.H.Y., Saez, I., Springhorn, A., Hoppe, T., Vilchez, D., Hansen, M., 2019. The autophagy receptor p62/SQST-1 promotes proteostasis and longevity in C. elegans by inducing autophagy. Nat. Commun. 10, 5648. https://doi.org/10.1038/s41467-019-13540-4.

Laitano, O., Garcia, C.K., Mattingly, A.J., Robinson, G.P., Murray, K.O., King, M.A., Ingram, B., Ramamoorthy, S., Leon, L.R., Clanton, T.L., 2020. Delayed metabolic dysfunction in myocardium following exertional heat stroke in mice. J. Physiol. 598, 967–985. https://doi.org/10.1113/JP279310.

Lee, I.Y., Lee, C.C., Chang, C.K., Chien, C.H., Lin, M.T., 2005. Sheng mai san, a Chinese herbal medicine, protects against renal ischaemic injury during heat stroke in the rat. Clin. Exp. Pharmacol. Physiol. 32, 742–748. https://doi.org/10.1111/j.1440-1681.2005.04259.x.

Leon, L.R., 2007. Heat stroke and cytokines. Prog. Brain Res. 162, 481–524. https://doi.org/10.1016/S0079-6123(06)62024-4.

Leon, L.R., Blaha, M.D., DuBose, D.A., 2006. Time course of cytokine, corticosterone, and tissue injury responses in mice during heat strain recovery. J. Appl. Physiol. 100 (1985), 1400–1409. https://doi.org/10.1152/japplphysiol.01040.2005.

Li, D., Yuan, J., Kopp, R., 2020. Escalating global exposure to compound heat-humidity extremes with warming. Res. Lett. 15 https://doi.org/10.1088/1748-9326/ab7d04.

Liu, Y., Wang, Z., Xie, W., Gu, Z., Xu, Q., Su, L., 2017. Oxidative stress regulates mitogenactivated protein kinases and cJun activation involved in heat stress and lipopolysaccharideinduced intestinal epithelial cell apoptosis. Mol. Med. Rep. 16, 2579–2587. https://doi.org/10.3892/mmr.2017.6859.

Liu, Z., Sun, X., Tang, J., Tang, Y., Tong, H., Wen, Q., Liu, Y., Su, L., 2011. Intestinal inflammation and tissue injury in response to heat stress and cooling treatment in mice. Mol. Med. Rep. 4, 437–443. https://doi.org/10.3892/mmr.2011.461.

Nicholson, J.K., Lindon, J.C., Holmes, E., 1999. Metabonomics': understanding the metabolic responses of living systems to pathophysiological stimuli via multivariate statistical analysis of biological NMR spectroscopic data. Xenobiotica 29, 1181–1189. https://doi.org/10.1080/004982599238047.

Pankiv, S., Clausen, T.H., Lamark, T., Brech, A., Bruun, J.A., Outzen, H., Overvatn, A., Bjorkoy, G., Johansen, T., 2007. p62/SQSTM1 binds directly to Atg8/LC3 to facilitate degradation of ubiquitinated protein aggregates by autophagy. J. Biol. Chem. 282, 24131–24145. https://doi.org/10.1074/jbc.M702824200.

Slimen, I.B., Najar, T., Ghram, A., Dabbebi, H., Ben Mrad, M., Abdrabbah, M., 2014. Reactive oxygen species, heat stress and oxidative-induced mitochondrial damage. A review. Int. J. Hyperth. 30, 513–523. https://doi.org/10.3109/02656736.2014.971446.

Stim, J., 1994. Maxwell & Kleeman's clinical disorders of fluid and electrolyte metabolism. JAMA 272, 245. https://doi.org/10.1001/jama.1994.03520030089043.

Tsai, Y.C., Lam, K.K., Peng, Y.J., Lee, Y.M., Yang, C.Y., Tsai, Y.J., Yen, M.H., Cheng, P.Y., 2016. Heat shock protein 70 and AMP-activated protein kinase contribute to 17-DMAG-dependent protection against heat stroke. J. Cell. Mol. Med. 20, 1889–1897. https://doi.org/10.1111/jcmm.12881.

Wang, C., Youle, R., 2016. Cell biology: form follows function for mitochondria. Nature 530, 288–289. https://doi.org/10.1038/530288a.

Wang, N.L., Chang, C.K., Liou, Y.L., Lin, C.L., Lin, M.T., 2005a. Shengmai San, a Chinese herbal medicine protects against rat heat stroke by reducing inflammatory cytokines and nitric oxide formation. J. Pharmacol. Sci. 98, 1–7. https://doi.org/10.1254/jphs.fp0050018.

Wang, N.L., Liou, Y.L., Lin, M.T., Lin, C.L., Chang, C.K., 2005b. Chinese herbal medicine, Shengmai San, is effective for improving circulatory shock and oxidative damage in the brain during heatstroke. J. Pharmacol. Sci. 97, 253–265. https://doi.org/10.1254/jphs.fp0040793.

Xia, Z., Huang, L., Yin, P., Liu, F., Liu, Y., Zhang, Z., Lin, J., Zou, W., Li, C., 2019. L-Arginine alleviates heat stress-induced intestinal epithelial barrier damage by promoting expression of tight junction proteins via the AMPK pathway. Mol. Biol. Rep. 46, 6435–6451. https://doi.org/10.1007/s11033-019-05090-1.

Yang, L., Duan, Z., Liu, X., Yuan, Y., 2018. N-acetyl-ʟ-cysteine ameliorates the PM2.5-induced oxidative stress by regulating SIRT-1 in rats. Environ. Toxicol. Pharmacol. 57, 70–75. https://doi.org/10.1016/j.etap.2017.11.011.

Zhang, K., Zhang, J., Wang, X., Wang, L., Pugliese, M., Passantino, A., Li, J., 2018. Cardioprotection of Sheng Mai Yin a classic formula on adriamycin induced myocardial injury in Wistar rats. Phytomedicine 38, 1–11. https://doi.org/10.1016/j.phymed.2017.09.001.

Zhang, P., Zheng, Y., Lv, Y., Li, F., Su, L., Qin, Y., Zeng, W., 2020. Melatonin protects the mouse testis against heat-induced damage. Mol. Hum. Reprod. 26, 65–79. https://doi.org/10.1093/molehr/gaaa002.

Zhang, W., Zhi, D., Ren, H., Wang, D., Wang, X., Zhang, Z., Fei, D., Zhu, H., Li, H., 2016. Shengmai formula ameliorates pathological characteristics in AD C. elegans. Cell. Mol. Neurobiol. 36, 1291–1302. https://doi.org/10.1007/s10571-015-0326-z.

Zhu, X., Long, D., Zabalawi, M., Ingram, B., Yoza, B.K., Stacpoole, P.W., McCall, C.E., 2020. Stimulating pyruvate dehydrogenase complex reduces itaconate levels and enhances TCA cycle anabolic bioenergetics in acutely inflamed monocytes. J. Leukocyte Biol. 107, 467–484. https://doi.org/10.1002/JLB.3A1119-236R.